A Journal of the Gesellschaft Deutscher Chemiker

Angewandte International Edition GDCh Chemie

www.angewandte.org

Accepted Article

Title: Zigzag Hopping Site Embedded Covalent Organic Frameworks Coating for Zn Anode

Authors: Can Guo, Xin Huang, Jianlin Huang, Xi Tian, Yuting Chen, Wenhai Feng, Jie Zhou, Qi Li, Yifa Chen, Shun-Li Li, and Ya-Qian Lan

To be cited as: *Angew. Chem. Int. Ed.* **2024**, e202403918

Link to VoR: https://doi.org/10.1002/anie.202403918

WILEY VCH

10.1002/anie.202403918

WILEY-VCH

RESEARCH ARTICLE

Zigzag Hopping Site Embedded Covalent Organic Frameworks Coating for Zn Anode

Can Guo[a]‡, Xin Huang[b]‡, Jianlin Huang[a], Xi Tian[b], Yuting Chen[a], Wenhai Feng[a], Jie Zhou[a], Qi Li[b], Yifa Chen [a]*, Shun-Li Li[a] & Ya-Qian Lan[a]*

[a] Dr. C. G., J. H., Y. C., W. F., J. Z., Prof. Y. C., Prof. S.-L. L. and Prof. Y.-Q. L.
School of Chemistry
South China Normal University
Guangzhou, 510006, P. R. China
[b] Dr. X. H., X. T. and Q. L.
School of Chemistry and Materials Science
Nanjing Normal University
South China Normal University
Nanjing 210023, P. R. China

E-mail: chyf927821@163.com; E-mail: yqlan@njnu.edu.cn; yqlan@m.scnu.edu.cn
Homepage : http://www.yqlangroup.com/

‡ Can Guo and Xin Huang contributed equally to this work

Supporting information for this article is given via a link at the end of the document.

Abstract: Precise design and tuning of Zn hopping/transfer sites with deeper understanding of the dendrite-formation mechanism is vital in artificial anode protective coating for aqueous Zn-ion batteries (AZIBs). Here, we probe into the role of anode-coating interfaces by designing a series of anhydride-based covalent organic frameworks (i.e., PI-DP-COF and PI-DT-COF) with specifically designed zigzag hopping sites and zincophilic anhydride groups that can serve as desired platforms to investigate the related Zn^{2+} hopping/transfer behaviours as well as the interfacial interaction. Combining theoretical calculations with experiments, the ABC stacking models of these COFs endow the structures with specific zigzag sites along the 1D channel that can accelerate Zn^{2+} transfer kinetics, lower surface-energy, homogenize ion-distribution or electric-filed. Attributed to these superiorities, thus-obtained optimal PI-DT-COF cells offer excellent cycling lifespan in both symmetric-cell (2000 cycles at 60 mA cm^{-2}) and full-cell (1600 cycles at 2 A g^{-1}), outperforming almost all the reported porous crystalline materials.

Introduction

The emergence and development of aqueous zinc-ion batteries (AZIBs) offer considerable opportunities for large-scale application and green energy storage devices to resolve the conflict between the energy crisis and environmental pollution.[1] The metallic Zn has been considered to be the most promising anode in AZIBs because of its distinctive merits, which include appropriate electrochemical potential (-0.76 V vs standard hydrogen electrode), intrinsic safety, high theoretical capacity (820 mAh g^{-1}), abundant reserves and low toxicity.[2] Nevertheless, one critical obstacle of AZIBs is their short lifespan that mainly caused by uncontrolled Zn dendrite formation and nonuniform Zn plating/stripping process, which leads to low Zn utilization and impeded electrochemical reaction kinetics.[3] The Zn generation at the interface between anode and electrolyte covers at least four consecutive processes during the Zn electroplating: Zn^{2+} diffusion, Zn^{2+} reduction, Zn nucleation, and Zn crystal growth.[4] The energy barrier stemmed from the Zn nucleus generation and crystal growth that should be broken in the above processes is caused by the electroplating conditions (e.g., anode affinity, electric field distribution at the anode-electrolyte interface, as well as anode flatness) need to overcome.[4] Theoretically, Zn^{2+} ions have a tendency to form nucleate at the preferred adsorption sites on the defective surface of the Zn anode. However, due to the much higher energy barrier of Zn nucleation compared to the Zn crystal growth on previously deposited nuclei, the successive deposition of Zn at the tip of Zn seed inevitably leads to uncontrolled growth of Zn dendrites.[4,5] To reduce the nucleation barrier and achieve the high performance of free-dendrite Zn anode, researchers have proposed several strategies including artificial anode protection coating, host architecting, electrolyte tuning, etc.[6] Among them, artificial anode protection coating (e.g., organic polymer-based coating, carbon materials, metal organic frameworks, metals and their compounds, etc.), as a promising alternative strategy for anode protection, possesses the functions of modulating the local electrical field around the Zn surface and shielding the direct contact between the Zn anode and H_2O molecules, thus impeding the growth of Zn dendrites and side reactions.[7] Nevertheless, the reported artificial anode protection coating on Zn anode is generally short in regular Zn^{2+} transport pathways as well as precise structures to modulate Zn hopping/transfer sites.[7,8] Besides, the deep understanding of the Zn^{2+} hopping/transfer, dendrite inhibition and plating/stripping behaviors as well as interfacial interaction in the artificial anode protection coating are urgently needed to investigate the structure-property relationships.

Recently, covalent organic frameworks (COFs), an emerging versatile of porous crystalline organic polymer materials with structural tunability, atomically ordered structures, ease of functionalization and high porosity, can serve as functional protection coatings to regulate the deposition behaviors of Zn^{2+} and achieve reversible dendrite-free Zn plating/stripping.[9] In this respect, it is speculated that COFs might be the potential

10.1002/anie.202403918
WILEY-VCH

RESEARCH ARTICLE

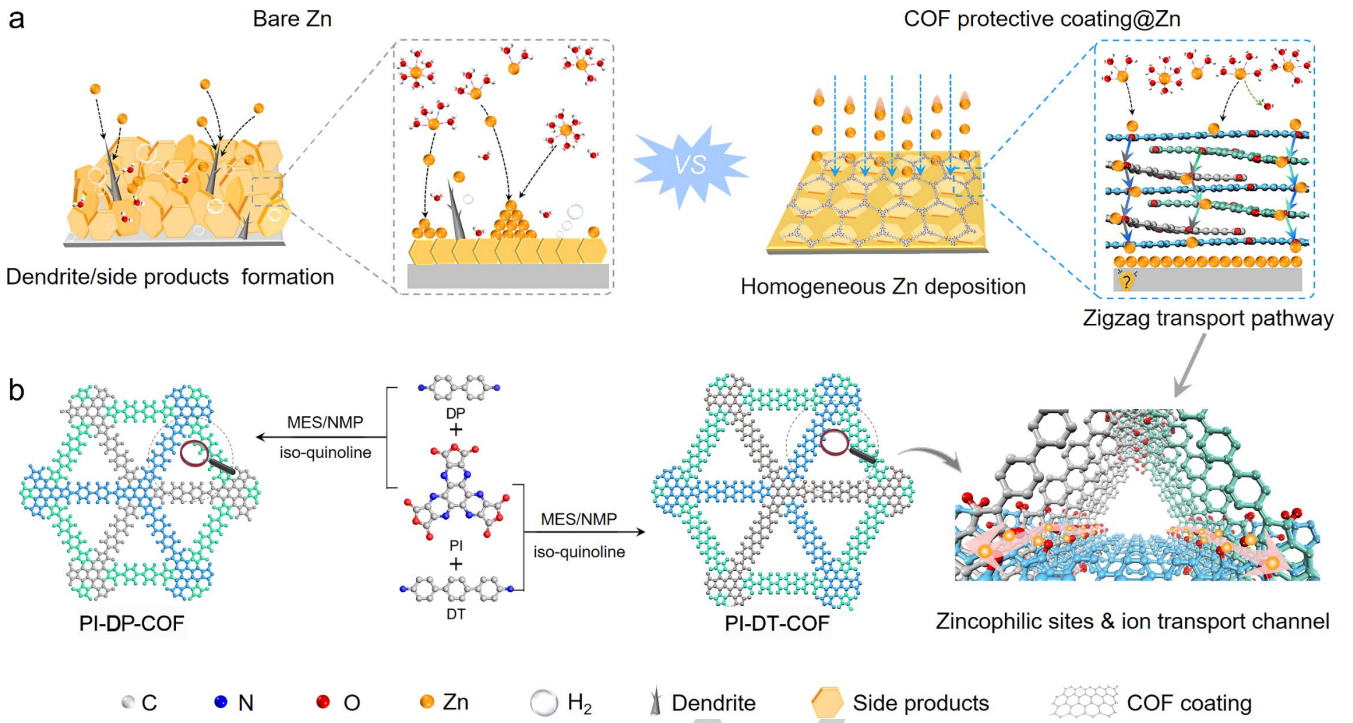

Figure 1. The schematic illustration of the advantages of anhydride-based COFs with zigzag sites for anode coating. **a** Schematic presentation of the Zn deposition behavior on bare Zn and anhydride-based COFs coated anode. **b** The synthesis and structure of PI-DT-COF and PT-DP-COF by the condensation of PI with DT and DP monomers, respectively.

candidates for the anode protection applications owing to the following advantages: 1) COFs with regular and predesigned channels can shorten the ion diffusion channels to facilitate Zn^{2+} migration within the coating and act as a molecular sieving barrier for electrolyte;[10] 2) the designable COFs structure can reasonable choice the organic building blocks with abundant zincophilic groups (such as -C=O, -C-F, -COOH, and -SO_3, etc.) to homogenize the electric field around the Zn anode surface;[10,11] 3) COFs might serve as water molecule sieving agents through physical/chemical interactions to destroy the coordination environment of the hydrated zinc ions and reduce dissolution barrier of Zn ions.[11a,11c] Nevertheless, only a few reports have employed COFs (i.e. DIP D, FCOF, PVC-Zn-AAn-COF@Zn, MNC@Zn, TpPa-SO_3H COF and 3D-COOH-COF) in AZIBs as anode protection coatings, and the mechanistic study of the Zn^{2+} diffusion within the COFs coating during the reversible plating/stripping process remains an immense challenge as far as we know.[10b,11] Besides, the interlayer stacking of 2D COFs also displays a profound influence on the COF isomers formation and variable interlayer stacking in COFs can result in different geometric structures, which will affect the electronic, catalytic or optic properties of COFs.[12] Therefore, the precise structure design of COFs with modulated Zn hopping/transfer sites to deeply understand the Zn^{2+} diffusion, dendrite inhibition and plating/stripping behaviors as well as interfacial interaction between anode and coating would be much essential for the development of high-performance AZIBs.

In order to gain deep insight into specific site functions and interfacial interaction of porous protection anode coating, we have prepared a series of anhydride-based COFs with specifically designed zigzag hopping sites and zincophilic anhydride groups (i.e. PI-DP-COF and PI-DT-COF) that can be applied as desired platforms to investigate the related Zn^{2+} hopping/transfer, dendrite inhibition, plating/stripping behaviors as well as interfacial interaction between anode and coating (Figure 1). Combining theoretical calculations with experiments, the ABC stacking model of anhydride-based COFs with specific zigzag sites can simultaneously realize the homogenous Zn^{2+} diffusion, shortened diffusion path and lower diffusion energy on the COFs-based platform to accelerate Zn^{2+} diffusion kinetics, lower surface-energy, homogenize ion-distribution or electric-filed. Notably, PI-DT-COF cells present an outstanding cycling lifespan in symmetric-cell and full-cells, outperforming almost all the reported porous crystalline materials.

Results and discussion

For the preparation of PI-DT-COF and PI-DP-COF, hexaazatriphenylenehexacarboxylic acid trianhydride (PI) as the vital precursor, was firstly prepared through multi-step organic synthesis procedures (Figure S1).[13] After that, PI-DT-COF and PI-DP-COF have been prepared through the connection of PI with 4,4''-diamino-p-terphenyl (DT) and 4,4'-diaminobiphenyl (DP) in Schiff base reactions at 180 °C for 7 days, respectively (Figures 1b, 2a and S2, details see Methods). Powder X-ray diffraction (PXRD) tests have been performed to clarify the crystal structure of the synthesized COFs. Specifically, the PXRD patterns of PI-DT-COF display obvious diffraction peak at 4.0°, which can be assigned to (210) faces (Figures 2a and S3). The experimental PXRD pattern of PI-DT-COF is accurately matched with the corresponding simulated ABC stacking model by structural simulation in BIOVIA Materials Studio 2019 (Figures 2a, S4 and Tables S1-3). It gives the refined unit lattice parameters (a = b = 44.07 Å, c = 6.50 Å) in the P_{63} space group with a negligible difference (R_p, 1.43% and R_{wp}, 2.07%), indicating the validity of the computational model (Figures 2a, S5 and Table S1). Meanwhile, the other models of PI-DT-COF including AA and AB

10.1002/anie.202403918

stacking models have also been simulated and fully optimized, while they do not match with the experimental PXRD patterns (Figures S6, 7 and Tables S2, 3). Besides, the stacking model of PI-DP-COF is similar to that of PI-DT-COF, which belongs to the ABC stacking rather than the AA or AB stacking (Figures 2b and S8-11). Interestingly, the ABC staggered stacking of PI-DT-COF leads to the zigzag arrangement of staggered nodes due to the abundant functional groups in the anhydride unit, in which the groups sites extend the out-of-plane of layers (Figures 1b and S5).[14] The orderly and abundantly arranged zincophilic groups (C=O and C=N) as well as favorable side distance of interlayer (the O-O distance, 3.6 and 6.7 Å, the N-N distance of 4.9, 5.8 and 7.1 Å) on the staggered nodes of ABC stacking along the *c* axis present the zigzag transport pathways for PI-DT-COF, which may promote the fast migration and hopping of Zn^{2+} ions.[11a,11f,14,15]

The Fourier transform infrared (FT-IR) and ^{13}C cross-polarization magic-angle-spinning nuclear magnetic resonance (^{13}C NMR) measurements have been conducted to confirm the formation of imine linkages of PI-DT-COF and PI-DP-COF. Taking PI-DT-COF for example, the disappearance of the anhydride (1685 cm^{-1}) and N-H (3302 and 3385 cm^{-1}) peaks are recognized as the monomers of PI and DT, respectively, revealing the successful preparation of PI-DT-COF from the two monomers (Figure 2c).[15,16] In addition, the C-N-C peak is observed at 1625 cm^{-1}, implying the existence of imine-linked network.[16] Similarly, the FT-IR spectra of anhydride, N-H and C-N-C of PI-DP-COF are close to that of PI-DT-COF, indicating that the presence of DP and PI ligands in PI-DP-COF (Figure S12). Moreover, the ^{13}C NMR spectrum of PI-DT-COF shows the signal of the carbonyl carbon of imide moieties (162.1 ppm), further implying the successful synthesis of PI-DT-COF (Figure 2d).[17] Besides, X-ray photoelectron spectroscopy measurements of PI, PI-DT-COF and PI-DP-COF exhibit the existence of C, O, and N peaks (Figures S13-15). Taking PI-DT-COF for instance, the main peaks at 284.7, 286.7 and 288.7 eV of the C 1s spectra can be assigned to C=C, C-N/C-O, and C=O, respectively (Figure S13b).[16b,18a] The O 1s spectrum reveals two peaks at 532.2 and 533.1 eV, which are attributed to O=C and O-H groups, respectively (Figure S13c).[16b,18a] The single peak of N 1s spectrum at 399.7 eV is detected, assigning to C-N-C groups (Figure S13d).[16b,18a] These results indicate the successful formation of imine-linked PI-DT-COF from the connection between PI and DT.

Scanning electron microscope (SEM) and transmission electron microscopy (TEM) tests have been used to investigate the morphology of the PI-DT-COF and PI-DP-COF. PI-DT-COF displays a kind of sphere morphology with an average diameter of ~200 nm in both SEM and TEM images (Figures 2e, f). The element mapping images reveal the homogeneous C, O, and N elements distribution over PI-DT-COF (Figure S16). In comparison, PI-DP-COF shows similar sphere morphology with PI-DT-COF in the SEM and TEM measurements (Figure S17). The chemical stability of PI-DT-COF has been also evaluated by soaking the sample in 1 M $ZnSO_4$ aqueous solution for 7 days. PXRD pattern of PI-DT-COF after soaking shows negligible changes, suggesting its excellent chemical stability (Figure S18).

Based on the aforementioned results, we have synthesized PI-DP-COF and PI-DT-COF with high porosity, zincophilic groups and chemical stability, which might serve as artificial protection coating to stabilize the Zn anodes. To examine the battery performance, PI-DP-COF@Zn and PI-DT-COF@Zn electrodes are fabricated by doctor casting onto the Zn surface based on PI-

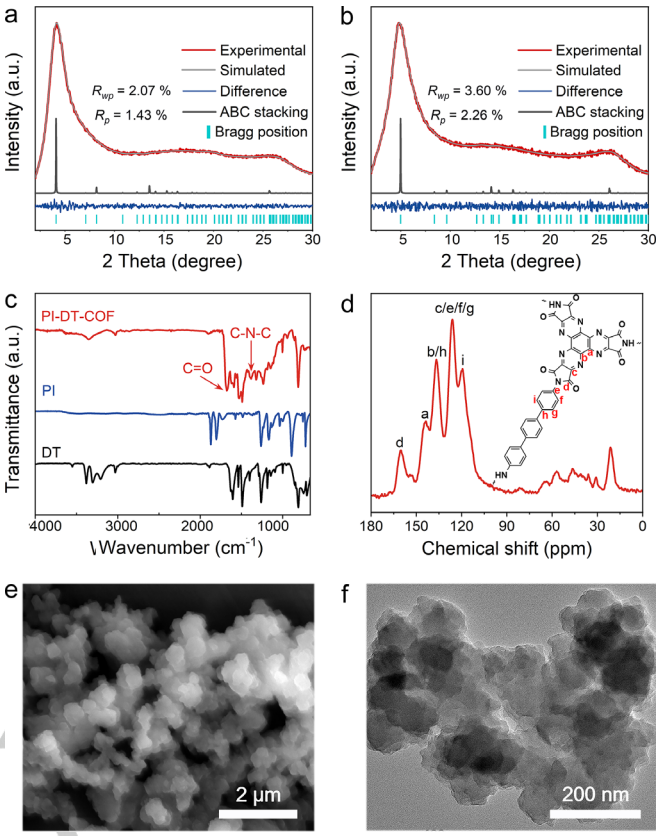

Figure 2. The preparation and characterization of PI-DT-COF and PT-DP-COF. **a** PXRD patterns of PI-DT-COF. **b** PXRD patterns of PI-DP-COF. **c** FT-IR spectra of PI-DT-COF, PI and DT. **d** The ^{13}C NMR spectrum of PI-DT-COF. **e, f** The morphology characterization of PI-DT-COF. **e** SEM image. **f** TEM image.

DP-COF and PI-DT-COF powders and polyvinylidene fluoride (PVDF) suspension, and further assembling into the cell for tests (details see Method). The side-view image of PI-DT-COF@Zn electrode presents a thickness of ~5 μm coating (Figure S19). To investigate the side reactions between the PI-DT-COF@Zn or bare Zn foil surface and electrolyte, the PI-DT-COF@Zn and bare Zn foil are immersed in 1 M $ZnSO_4$ electrolyte. The PI-DT-COF@Zn surface remains unchanged after 7 days, revealing the high chemical stability of PI-DT-COF@Zn toward the aqueous electrolyte (Figure S20a). In contrast, the bare Zn foil surface is slightly corroded after 3 days, accompanying with the color changed from bright to gray, demonstrating the extremely unstable in electrolyte (Figure S20b). Besides, compared with the bare Zn anode, the increased wettability of PI-DT-COF@Zn anode would make the electrolyte to be more infiltration over the surface (Figure S21). To obtain further insight into the positive impact of the PI-DT-COF coating, the corrosion resistance on the PI-DT-COF@Zn and bare Zn has been assessed by linear polarization measurements (Figure S22). Notably, the PI-DT-COF@Zn anode delivers the lower corrosion current density (2.21 mA cm^{-2}) than the bare Zn anode (2.95 mA cm^{-2}), indicating the diminished Zn corrosion of PI-DT-COF coating in aqueous electrolytes.[11d,18] The superb corrosion resistance of PI-DT-COF@Zn proves that the PI-DT-COF coating successfully prevents the direct contact between the electrolyte and bare Zn anode surface, hence mitigating the interfacial side reactions.

To evaluate the electrochemical performance of PI-DT-COF@Zn, PI-DP-COF@Zn and bare Zn anodes during the Zn plating/stripping process, corresponding symmetric batteries

10.1002/anie.202403918

RESEARCH ARTICLE

have been assembled and tested. The rate performance of PI-DT-COF@Zn and bare Zn symmetric batteries are carried out at various current densities with 1 mAh cm^{-2} (Figure 3a). When the current density increases from 1 to 20 mA cm^{-2}, the PI-DT-COF@Zn symmetric cell displays a steadier voltage profile with lower voltage hysteresis (hysteresis steadily increasing from 14.5 to 102.0 mV), whereas bare Zn symmetric cell abruptly fails at 20 mA cm^{-2}, showing the PI-DT-COF coating plays a crucial role in enhancing rate performance (Figure 3a). The exchange current density linked with the Zn deposition process may be determined based on the current density and overpotential from rate performance to assess the kinetics of the PI-DT-COF@Zn and are Zn electrodes during Zn plating/stripping process (Figures 3a, S23). PI-DT-COF@Zn has a high exchange current density of 7.51 mA than that of bare Zn (3.96 mA), demonstrating the PI-DT-COF coating can homogenize Zn^{2+} deposition and boost Zn deposition kinetics.[19] Besides, the Zn^{2+} transference number of PI-DT-COF@Zn symmetric battery (0.76) is much higher than that of bare Zn (0.60), indicating the much more favored Zn^{2+} ion transfer in PI-DT-COF coating (Figure S24). These results suggest that PI-DT-COF coating can alleviate interface concentration distribution, reduce Zn^{2+} deposition barrier and homogenize Zn plating/stripping, thus inhibiting the dendrite growth.[11c] The influence of the Zn^{2+} transport property of symmetric cells with the PI-DT-COF coating shows the invertibility and stability during the Zn plating/stripping process. Beyond that, *ex-situ* SEM characterizations are conducted to analyze the influence of PI-DT-COF coating for Zn deposition morphology (Figure S25). At different current densities (1, 2 and 3 mA cm^{-2}), the PI-DT-COF@Zn electrode surface displays uniform and smooth morphology and there is no inhomogeneous protuberance identified (Figures S25a-c). Contrastingly, the bare Zn shows the protuberance and Zn nanosheets of the bumpy surface at 1 mA cm^{-2} with 1 mAh cm^{-2} (Figure S25d). Note that as the current density further increases to 3 mA cm^{-2} with 3 mAh cm^{-2}, the Zn protrusions turn larger, demonstrating the tip-induced and uncontrolled growth of Zn dendrite for the bare Zn anode (Figure S25f).

The PI-DT-COF@Zn symmetric battery presents a steady polarization voltage (~48 mV) and cycling life over 500 h at 5 mA cm^{-2} with 1 mAh cm^{-2}, which is nearly four times of bare Zn symmetric battery (Figure S26). In contrast, the PI-DP-COF@Zn and bare Zn symmetric batteries exhibit an abrupt failure after 386 and 130 h, respectively, because of the uncontrolled internal short circuit caused by dendrites. To prove the importance of PI-DT-COF coating, PVDF@Zn symmetric battery is assembled and

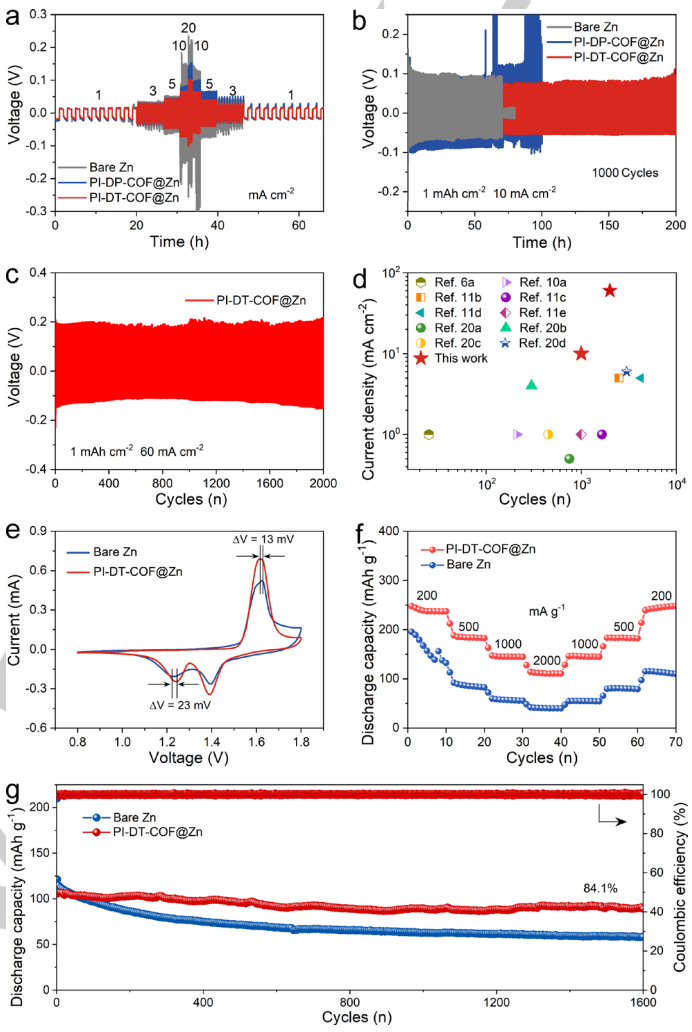

Figure 3. Electrochemical performance of PI-DT-COF@Zn, PI-DP-COF@Zn and bare Zn symmetric batteries. **a** Rate performance of symmetric batteries at different current densities. **b** Cycling performance of symmetric batteries at 10 mA cm^{-2}. **c** Long-cycling performance of PI-DT-COF@Zn symmetric battery at 60 mA cm^{-2}. **d** Comparison of the cycle life of PI-DT-COF@Zn symmetrical cell and those of previously reported anode modification, electrolyte optimization under various current densities. **e** The CV curves of the PI-DT-COF@Zn and bare Zn full cells. **f** Rate performance of the full cells. **g** Cycling performance of the full cells at 2000 mA g^{-1}.

10.1002/anie.202403918

displays severe voltage fluctuation and polarization at 140 h, demonstrating the positive effect of PI-DT-COF on preventing dendrite growth (Figure S27). To verify the vital role of anhydride group, TP-DT-COF, an iso-reticular COF to PI-DT-COF with the only difference in PI and TP ligand, is also assembled into TP-DT-COF@Zn battery under the same assembled conditions of PI-DT-COF@Zn battery (Figure S2). TP-DT-COF@Zn symmetric cell shows the poor cycling stability (~200 h) and low voltage polarization (89.0 mV) at 5 mA cm^{-2}, revealing the existence of PI in the PI-DT-COF coating can efficiently promote Zn^{2+} transport ability during the reversible Zn plating/stripping process (Figure S28).

In general, increasing current density might lead to the uneven electric field at the anode and electrolyte interface, which would then encourage unfavorable nucleation. When the current density is expended to 10 mA cm^{-2}, the PI-DT-COF@Zn symmetric battery can continue to maintain excellent cycling stability of > 200 h, which is substantially longer than the PI-DP-COF@Zn (~58 h) and bare Zn (~70 h) symmetric batteries (Figure 3b). Compared to PI-DP-COF@Zn, TP-DT-COF@Zn, PVDF@Zn, and bare Zn symmetric batteries, PI-DT-COF symmetric batteries present the most stable voltage profiles and lowest overpotential, which proves the PI-DT-COF coating is exceptionally effective component for stabilizing the Zn plating/stripping owing to its unique zigzag structure, fast Zn^{2+} migration, outstanding Zn deposition kinetics and corrosion prohibition ability. After increasing the current density to 40 mA cm^{-2}, the PI-DT-COF@Zn symmetric battery can still run for 1000 cycles of cycling (Figure S29). Importantly, the PI-DT-COF@Zn symmetric battery displays a stable overpotential and remarkable long-cycling life over 2000 cycles at an ultra-high current density of 60 mA cm^{-2} (Figure 3c). Impressively, the distinguished electrochemical reversibility of PI-DT-COF anode surpasses the most recently reported results of AZIBs based on anode modification (Figure 3d and Table S7).[6b,10a,11b-11e,20] The morphology images of the PI-DT-COF@Zn and bare Zn anodes after 100 cycles are also used to clarify the importance of PI-DT-COF in the cycling process by SEM tests (Figure S30). The PI-DT-COF@Zn anode equipped with Zn^{2+} modulation coating exhibits the smooth, compact surface devoid of any protruding filaments (Figure S30a). By contrast, the surface of bare Zn presents typical mossy and fluffy structure with lengthy and disordered acicular Zn, suggesting the uncontrolled growth of Zn dendrite and the risk of a short circuit of battery by penetrating separator (Figure S30b). Besides, the nucleation overpotential tests of PI-DT-COF@Cu and bare Cu electrodes display that PI-DT-COF@Cu possesses the lower nucleation overpotential to guide uniform Zn deposition (Figure S31). Coulombic efficiency (CE) of PI-DT-COF@Cu and bare Cu anodes is a crucial factor to assess the reversible Zn metal anode during repeated Zn plating/stripping. PI-DT-COF@Cu symmetric cell sustains a high average CE of 99% after 160 cycles at 10 mA cm^{-2} with 5 mAh cm^{-2}, indicating prominent reversibility of Zn plating/stripping (Figure S32). In addition, bare Cu foil symmetric cell shows the fluctuant voltage after 60 cycles and then rapid failure of battery, suggesting the dendrite growth and side reactions occurrence. The higher CE of PI-DT-COF@Cu symmetric cell indicates the PI-DT-COF coating aids in delaying side reactions and impeding the formation of dendrite growth.[21]

Inspired by the excellent electrochemical reversibility of the designed PI-DT-COF@Zn anode, PI-DT-COF and bare Zn full batteries are assembled and assessed by matching the MnO_2 cathodes based on aqueous electrolyte (1 M $ZnSO_4$ + 0.15 M $MnSO_4$) to confirm the potential of PI-DT-COF@Zn anode for practical applications.[11d] The cyclic voltammetry (CV) profiles of PI-DT-COF@Zn and bare Zn full batteries exhibit the similar shape at a scan rate of 0.2 mV s^{-1} (Figures 3e and S33). Notably, the PI-DT-COF@Zn full battery exhibits a higher peak current and narrower voltage gap between redox peaks, identifying decreased electrochemical polarization and corrosion passivation to improve the Zn^{2+} ions transfer kinetics and reversibility of electrochemical process (Figure 3e). Bsides, the PI-DT-COF@Zn full battery exhibits the higher rate performance than bare Zn full battery (Figure 3f). Furthermore, the long-term cycling stability of PI-DT-COF@Zn full battery at 2000 mA g^{-1} achieves an impressive reversible discharge capacity of 89.8 mAh g^{-1} after 1600 cycles, which suggests the superior cycling stability (Figure 3g). These results further confirm PI-DT-COF coating can effectively impede Zn dendrite growth and corrosion to prolong the superb cycling lifespan and rate performance. In addition, the flexible PI-DT-COF@Zn full battery can effectively power up a light emitting diode, demonstrating the potential application prospect of PI-DT-COF@Zn full battery in portable electronic devices (Figure S34).

The distribution of the electric field at the anode surface has a considerable influence on the Zn nucleation and deposition. To demonstrate the influence of PI-DT-COF coating for the Zn nucleation kinetics on anode-electrolyte interface, current density and electric field distribution have been studied by COMSOL Multiphysics simulation based on the simplified structure simulation models of the PI-DT-COF@Zn and bare Zn anodes. The simulation results of PI-DT-COF@Zn anode display the uniform current density and electric field distribution at the interface, which results in the even Zn^{2+} flux distribution, thereby guiding the homogenous Zn deposition and dendrite-free morphology (Figures 4a, c and S35).[6b,18a,22] In contrast, the bare Zn anode displays an obviously inhomogeneous electric field distribution, which causes the random deposition and nucleation of Zn^{2+} on the anode surface to form irregular protuberances and enhance the local electric field on the tips (Figures 4b, d and S36).[6b,22a,23] These protuberances enhance the local electric field stemming from the nucleation of the excessive Zn^{2+} ions to the tips, thereby promoting the Zn dendrites formation and growth.[22a,23] Besides, the uneven electric field would cause local charge to gather at the tip, thus producing the tip effect, which is confirmed by 2D/3D laser topographic images (Figures 4e, f and S37). Compared to bare Zn surface, the PI-DT-COF@Zn anode surface shows the homogeneous and smooth Zn deposition after 100 cycles at 10 mA cm^{-2}.[21] Later on, Kelvin probe force microscopy (KPFM) and atomic force microscopy (AFM) are introduced to trace the surface evenness and potential of PI-DT-COF@Zn and bare Zn anodes after 100 cycles at 10 mA cm^{-2}. PI-DT-COF@Zn anode displays a flat surface morphology and low surface potential fluctuations than that of bare Zn anode (Figures 4g, h and S38).[6b,22a]

10.1002/anie.202403918

RESEARCH ARTICLE

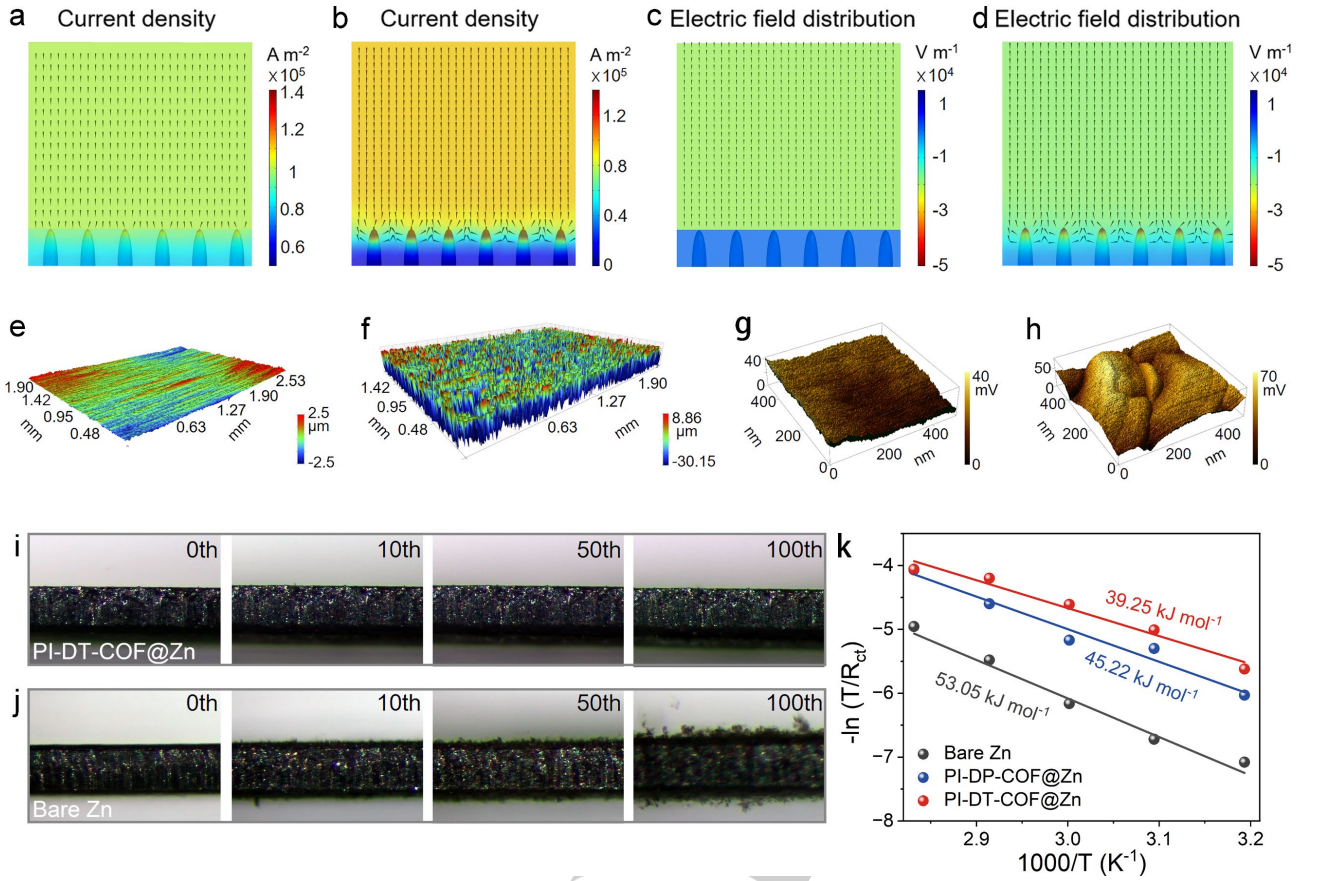

Figure 4. Mechanism study of Zn deposition behaviors on PI-DT-COF@Zn. **a** The current density distribution for PI-DT-COF@Zn anode. **b** The current density distribution for bare Zn anode. **c** The relative electric field distribution simulation for PI-DT-COF@Zn anode. **d** The relative electric field distribution simulation for bard Zn anode. **e, f** 3D laser optical images of the PI-DT-COF@Zn and bare Zn anodes surface after 100 cycles at 10 mA cm^{-2}. **g, h** KPFM images of the surface of PI-DT-COF@Zn and bare Zn anodes after 100 cycles. **i, j** *In-situ* optical investigations of the Zn plating process for the PI-DT-COF@Zn **i** and bare Zn anode **j** at various cycles. **k** The calculation of activation energies of different anodes based on the Arrhenius curves.

In addition, the optical morphological evaluation of Zn deposition process has been *in-situ* monitored through optical microscopy imaging utilizing a transparent symmetric batteries device at 10 mA cm^{-2} with 1 mAh cm^{-2} (Figures 4i, j). The PI-DT-COF@Zn anode shows a smooth surface and invisible dendrites generation during the whole plating (Figure 4i). In comparison, a number of visible spots of bare Zn anode appear after 10 cycles (Figure 4j). After 100 cycles, the larger uncontrolled Zn dendrites ultimately spread on the bare Zn anode surface, raising the possibility of short-circuit dangers as well as other safety concerns. The porous PI-DT-COF coating may successfully prevent the formation of Zn dendrites, as shown by both SEM and optical microscope monitoring. Besides, the inhibition ability of PI-DT-COF@Zn symmetric cell has been verified by battery-gas chromatography mass spectrometry and linear sweep voltammetry tests. The H_2 evolution flux of PI-DT-COF@Zn and bare Zn symmetric cell using two electrode system is *ex-situ* examined at 10 mA cm^{-2} with 1 mAh cm^{-2} through battery-gas chromatography mass spectrometry. The H_2 evolution flux of the PI-DT-COF@Zn symmetric cell displays the tiny quantity of H_2 evolution (8 μmol h^{-1} cm^{-2} after 30 cycles) and is >10 times higher than that of bare Zn symmetric cell (80 μmol h^{-1} cm^{-2} after 30 cycles), demonstrating PI-DT-COF coating with the inhibition ability of H_2 evolution (Figure S39). The result of linear sweep voltammetry presents that the hydrogen evolution potential of PI-DT-COF@Zn symmetric cell is more than that of bare Zn symmetric cell, demonstrating that PI-DT-COF protection coating can alleviate the H_2 evolution reaction to some extent (Figure S40). Meanwhile, the Gibbs free energy for H_2 adsorption on the PI-DT-COF@Zn interface (1.15 eV) is almost twice as high as that of bare Zn (0.55 eV) based on density functional theory (DFT) calculations, which suggests that PI-DT-COF coating can limit to H_2 evolution to some extent (Figure S41).[24] Beyond that, the Zn^{2+} ion transfer resistance of PI-DT-COF coating in Zn plating process has been investigated through the electrochemical impedance spectroscopy in symmetric cell at different temperatures between 30 °C and 80 °C (Figures 4k and S42). The activation energy (E_a) of Zn^{2+} ion transfer and desolvation effect can be evaluated according to Arrhenius equation law (Figure 4k). The E_a of PI-DT-COF@Zn symmetric cell (39.25 kJ mol^{-1}) is lower than those of PI-DP-COF@Zn (45.22 kJ mol^{-1}) and bare Zn (53.05 kJ mol^{-1}) symmetric cells by the relevant calculated results, which verifies that the PI-DT-COF coating can largely improve the Zn^{2+} transfer kinetics.[22b]

As an artificial protection coating for the Zn anode, the Zn^{2+} migration behavior would determine the kinetics of the Zn plating/stripping process. To clarify the zincophilicity and desolvation effects of PI-DT-COF coating, DFT calculations have been carried out based on the calculated models (Figures 5a-c and S43-49). The high absorption energy of PI-DT-COF@Zn (-3.68 vs -1.25 eV of H_2O@Zn) indicates that the protection coating displays the strong zincophilic ability to Zn foil and accelerates

10.1002/anie.202403918

Zn^{2+} desolvation process (Figures 5a, b and S45).[24] Meanwhile, the calculated Zn^{2+} adsorption energy of the PI-DT-COF (-1.86 eV) is higher than that of bare Zn (-0.64 eV), indicating that PI-DT-COF coating has the strong zincophilic ability at the anode-electrolyte interface because of the existence of -C=O groups, which can improve the Zn^{2+} capture and transfer ability at the PI-DT-COF@Zn interface during the plating/stripping process (Figures 5c and S47, 48).[11c,18a] Besides, the absorption energy of Zn^{2+}-PI-DT-COF@Zn is much stronger than that of H_2O-PI-DT-COF (-0.18 eV), implying the PI-DT-COF coating can efficiently accelerate Zn^{2+} desolvation process (Figure S49).[18a]

To gain a thorough insight into the Zn^{2+} migration, the transport mechanism of PI-DT-COF has been verified through a machine learning potential based molecular dynamics (MD) simulation and DFT calculations. The calculation result of the electrostatic potential (ESP) of PI-DT-COF shows that the electronegative part is mainly concentrated on the -C=O (Figure S50).[11c,17a] Thus, the strong interaction between Zn^{2+} with positive charge and -C=O group of PI-DT-COF has been investigated, and the optimized adsorption configurations of Zn^{2+} adsorbed on the PI-DT-COF and bare Zn foil surface have been provided (Figure S51).[17a,18a,25] The differential charge density distribution and associated 2D contour map of the optimized PI-DT-COF@Zn surface by DFT calculations display the high electronegativity of -C=O can distinctly modify the charge distribution and result in the unbalanced charge distribution at the interface between PI-DT-COF platform and Zn foil (Figure 5d).[19,20a] These results can determine the transport site of Zn^{2+}, accelerate the diffusion of Zn^{2+} at the PI-DT-COF@Zn platform and improve the adhesion between the PI-DT-COF coating and the Zn foil, which agrees with the absorption energy results.[17a,18a,19,25] Furthermore, the snapshots of Zn^{2+} solvation structures in PI-DT-COF@Zn and bare Zn anodes have been achieved using MD simulation (Figures 5e, f and S52). Compared to that on the surface of bare Zn anode, the Zn^{2+} on the PI-DT-COF@Zn anode-electrolyte interface has been more evenly captured by PI-DT-COF coating as opposed to water owing to the stronger absorption between Zn^{2+} and PI-DT-COF (Figures 5e, f and Videos S1, S2).[21,26] Radial distribution functions (RDFs) based on MD simulation further support the structure modification of the hydrated Zn^{2+} at the PI-DT-COF@Zn and bare Zn anodes interface (Figure 5g). The results show that the PI-DT-COF@Zn model contemporaneously delivers a wider Zn^{2+} distribution in contrast to that of bare Zn model, demonstrating the considerably uniform

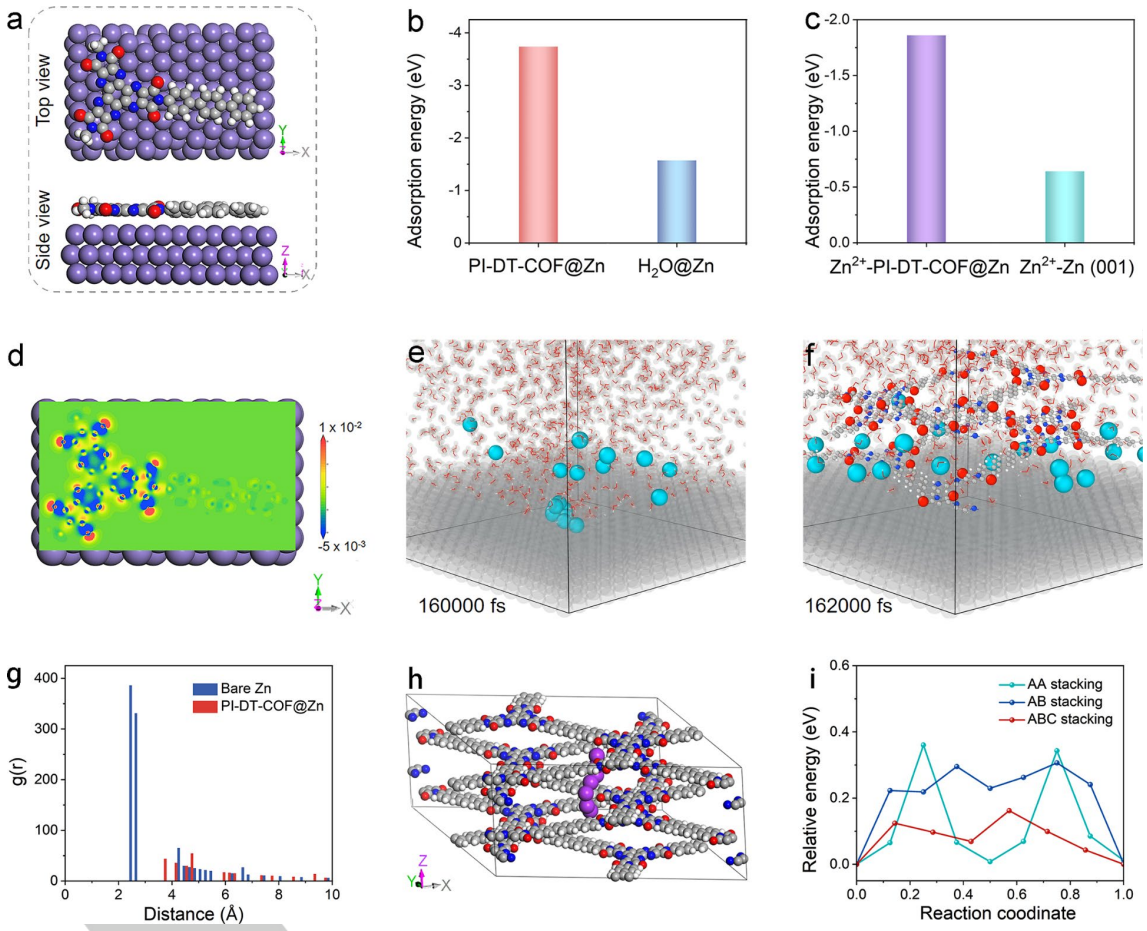

Figure 5. Investigation of the Zn^{2+} transport mechanism and Zn^{2+} solvation structure. **a, b** Theoretical calculations models of PI-DT-COF adsorbed on Zn foil **a** and the corresponding calculated adsorption energies **b**. **c** The adsorption energies of Zn^{2+} on PI-DT-COF and bare Zn foil. **d** Electron density difference map at the PI-DT-COF@Zn interphase. **e** Snapshots of Zn deposition on the bare Zn anode surface. **f** Snapshots of Zn deposition on the PI-DT-COF@Zn anode surface. **g** Corresponding RDFs plots of Zn deposition on PI-DT-COF@Zn and bare Zn anodes surface. **h** The diffusion paths for Zn^{2+} to migrate on ABC stacking model of PI-DT-COF. **i** The calculated activation energy of Zn^{2+} migration for the different stacking models of PI-DT-COF@Zn anode along specific pathways stemmed from NEB by MD simulation.

10.1002/anie.202403918

Zn^{2+} deposition in the PI-DT-COF@Zn model.[21,26,27] The Zn^{2+} diffusion coefficient value of Zn^{2+} in PI-DT-COF coating (0.042 A^2/ps^{-1}) by MD simulation is one order of magnitude larger than that of bare Zn ($1.88E^{-3}$ A^2/ps^{-1}) in the aqueous electrolyte (Figures 5e, f, S53 and Videos S1, S2).[28]

Beyond that, the Zn^{2+} diffusion energy barriers along the *c*-axis on the PI-DT-COF@Zn, TP-DT-COF@Zn and bare Zn surface have been calculated to reveal the Zn^{2+} diffusion mechanism by climb-image nudged elastic band (CI-NEB) calculations (Figures 5h, i and S54-57). The calculated migration energy barrier for Zn^{2+} diffusion on ABC stacking PI-DT-COF@Zn platform (0.16 eV) is lower than that of AB (0.31 eV) and AA (0.39 eV) stacking models (Figures 5h, S54 and 56). The MD simulations further demonstrate Zn^{2+} with positive charge jumps through the O atom sites and transmits along the *c*-axis permutation channel during the plating/stripping process (Figure S58).[26a,29] ABC stacking model of PI-DT-COF shortens the transport path and facilitates the transmission of Zn^{2+}, which is consistent with the ESP calculation results. Besides, the calculated energy barrier for Zn^{2+} diffusion on TP-DT-COF@Zn platform and bare Zn surface are 0.87 and 0.01 eV, respectively (Figures S56, 57). The ultralow calculated diffusion energy barrier of the bare Zn (001) surface reveals essentially instantaneous and unhindered Zn^{2+} diffusion, thereby leading to the resultant tip effect and uncontrolled Zn dendrites growth.[26a,29a] Therefore, PI-DT-COF in the ABC stacking model can facilitate the Zn^{2+} diffusion kinetics in the interface of anode and coating, impede Zn^{2+} agglomeration and homogenize the Zn^{2+} flux, which can be ascribed to the abundant and readily available zigzag transport sites that can impart PI-DT-COF@Zn anode with the ability of Zn dendrite growth inhibition.

Conclusion

In summary, to investigate the related Zn^{2+} hopping/transfer, dendrite inhibition, plating/stripping behaviours as well as interfacial interaction between anode and coating, a series of anhydride-based COFs (i.e., PI-DP-COF and PI-DT-COF) with zincophilic anhydride groups and specifically designed zigzag hopping sites have been synthesized as desired platforms. Combining theoretical calculations with experiments, the ABC stacking model of anhydride-based COFs with specific zigzag sites can simultaneously realize the continuous Zn^{2+} diffusion and short diffusion path on the COFs-based platform to accelerate Zn^{2+} transfer kinetics, lower surface-energy, homogenize ion-distribution or electric-field. Attributed to these superiorities, thus-obtained optimal PI-DT-COF cells offer excellent cycling lifespan in both symmetric-cell (2000 cycles at 60 mA cm^{-2}) and full-cell (1600 cycles at 2000 mA g^{-1}), outperforming almost all the reported porous crystalline materials. This work with specifically designed zigzag site and well-studied interfacial interaction between anode and coating might facilitate the development of porous crystalline materials in protective anode-coating field.

Supplemental Information includes 58 Figures and 7 Tables

Acknowledgements

This work was financially supported by the NSFC (Grants no. 22225109, 22071109, and 22171139), Natural Science Foundation of Guangdong Province (Grants no. 2023B1515020076), and Open Fund of Energy and Materials Chemistry Joint Laboratory of SCNU and TINCI.

Conflict of Interest

The authors declare no conflict of interest.

Keywords: covalent organic frameworks • Zigzag Site • Zn anode • Coating

References

[1] a) R. F. Service, *Science* **2021**, *372*, 890-891; b) N. Kittner, F. Lill, D. M. Kammen, *Nat. Energy* **2017**, *2*, 17125.
[2] a) S. Liu, R. Zhang, J. Mao, Y. Zhao, Q. Cai, Z. Guo, *Sci. Adv.* **2022**, *8*, eabn5097; b) R. Wang, M. Yao, M. Yang, J. Zhu, J. Chen, Z. Niu, *Proc. Natl. Acad. Sci. U.S.A.* **2023**, *120*, e2221980120; c) F. Wang, O. Borodin, T. Gao, X. Fan, W. Sun, F. Han, A. Faraone, J. A. Dura, K. Xu, C. Wang, *Nat. Mater.* **2018**, *17*, 543-549.
[3] H. Yu, Y. Zeng, N. W. Li, D. Luan, L. Yu, X. W. D. Lou, *Sci. Adv.* **2022**, *8*, eabm5766.
[4] Z. Yi, G. Chen, F. Hou, L. Wang, J. Liang, *Adv. Energy Mater.* **2021**, *11*, 2003065.
[5] a) R. Qin, Y. Wang, L. Yao, L. Yang, Q. Zhao, S. Ding, L. Liu, F. Pan, *Nano Energy* **2022**, *98*, 107333; b) J. Yang, B. Yin, Y. Sun, H. Pan, W. Sun, B. Jia, S. Zhang, T. Ma, *Nano Micro Lett.* **2022**, *14*, 42-47.
[6] a) Z. Wang, J. Huang, Z. Guo, X. Dong, Y. Liu, Y. Wang, Y. Xia, *Joule* **2019**, *3*, 1289-1300; b) P. Xue, C. Guo, L. Li, H. P. Li, D. Luo, L. C. Tan, Z. W. Chen, *Adv. Mater.* **2022**, *34*, e2110047; c) J. Hao, L. Yuan, C. Ye, D. Chao, K. Davey, Z. Guo, S.-Z. Qiao, *Angew Chem. Int. Ed.* **2021**, *60*, 7366-7375.
[7] H. Yu, Y. Chen, W. Wei, X. Ji, L. Chen, *ACS Nano* **2022**, *16*, 9736-9747.
[8] L. T. Hieu, S. So, I. T. Kim, J. Hur, *Chem. Eng. J.* **2021**, *411*, 128584.
[9] a) C. S. Diercks, O. M. Yaghi, *Science* **2017**, *355*, 6328; b) C. Wei, L. Tan, Y. Zhang, K. Zhang, B. Xi, S. Xiong, J. Feng, Y. Qian, *Acs Nano* **2021**, *15*, 12741-12767.
[10] a) J. H. Park, M. J. Kwak, C. Hwang, K. N. Kang, N. Liu, J. H. Jang, B. A. Grzybowski, *Adv. Mater.* **2021**, *33*, 2101726; b) C. Guo, J. Zhou, Y. Chen, H. Zhuang, J. Li, J. Huang, Y. Zhang, Y. Chen, S.-L. Li, Y.-Q. Lan, *Angew Chem. Int. Ed.* **2023**, *62*, e202300125.
[11] a) C. Guo, J. Zhou, Y. Chen, H. Zhuang, Q. Li, J. Li, X. Tian, Y. Zhang, X. Yao, Y. Chen, S.-L. Li, Y.-Q. Lan, *Angew. Chem. Int. Ed.* **2022**, *61*, e202210871; b) J. Zhao, Y. Ying, G. Wang, K. Hu, Y. D. Yuan, H. Ye, Z. Liu, J. Y. Lee, D. Zhao, *Energy Storage Mater.* **2022**, *48*, 82-89; c) Y. Wang, Z. Deng, B. Luo, G. Duan, S. Zheng, L. Sun, Z. Ye, J. Lu, J. Huang, Y. Lu, *Adv. Funct. Mater.* **2022**, *32*, 2209028; d) Z. Zhao, R. Wang, C. Peng, W. Chen, T. Wu, B. Hu, W. Weng, Y. Yao, J. Zeng, Z. Chen, P. Liu, Y. Liu, G. Li, J. Guo, H. Lu, Z. Guo, *Nat. Commun.* **2021**, *12*, 6606; e) K. Wu, X. Shi, F. Yu, H. Liu, Y. Zhang, M. Wu, H.-K. Liu, S.-X. Dou, Y. Wang, C. Wu, *Energy Storage Mater.* **2022**, *51*, 391-399; f) Z. Mei, H. Li, G. Wang, Y. Mao, Y. Xu, J. Guo, Q. Li, H. Li, W. Li, Y. Tang, X. Liang, *Appl. Surf. Sci.* **2023**, *615*, 156324.
[12] S. Yang, X. Li, Y. Qin, Y. Cheng, W. Fan, X. Lang, L. Zheng, Q. Cao, *ACS Appl. Mater. Interfaces* **2021**, *13*, 29471-29481.
[13] a) K. Kanakarajan, A. W. Czarnik, *J. Org. Chem.* **1986**, *51*, 5241-5243; b) J. T. Rademacher, K. Kanakarajan, A. W. Czarnik, *Synthesis*, **1994**, 378-380.
[14] Wu, X. Han, Y. Liu, Y. Liu, Y. Cui, *J. Am. Chem. Soc.* **2018**, *140*, 16124-16133.
[15] X. Yang, L. Gong, X. Liu, P. Zhang, B. Li, D. Qi, K. Wang, F. He, J. Jiang, *Angew Chem. Int. Ed.* **2022**, *61*, e202207043.
[16] J. Maschita, T. Banerjee, G. Savasci, F. Haase, C. Ochsenfeld, B. V. Lotsch, *Angew Chem. Int. Ed.* **2020**, *59*, 15750-15758.

10.1002/anie.202403918

[17] a) F. Ye, Q. Liu, H. Dong, K. Guan, Z. Chen, N. Ju, L. Hu, *Angew Chem. Int. Ed.* **2022**, *61*, e202214244; b) H. Duan, K. Li, M. Xie, J.-M. Chen, H.-G. Zhou, X. Wu, G.-H. Ning, A. I. Cooper, D. Li, *J. Am. Chem. Soc.* **2021**, *143*, 19446-19453.

[18] a) P. Wang, S. Liang, C. Chen, X. Xie, J. Chen, Z. Liu, Y. Tang, B. Lu, J. Zhou, *Adv. Mater.* **2022**, *34*, 2202733; b) X Li, Z. Chen, P. Ruan, X. Hu, B. Lu, X. Yuan, S. Tian, J. Zhou, *Nanoscale*, **2024**, *16*, 2923-2930; c) J. Li, Z. Liu, S. Han, P. Zhou, B. Lu, J. Zhou, Z. Zeng, Z. Chen, J. Zhou, *Nano Micro Lett.* **2022**, *15*, 237.

[19] L. Hong, X. Wu, C. Ma, W. Huang, Y. Zhou, K.-X. Wang, J.-S. Chen, *J. Mater. Chem. A* **2021**, *9*, 16814-16823.

[20] a) H. Yang, Z. Chang, Y. Qiao, H. Deng, X. Mu, P. He, H. Zhou, *Angew Chem. Int. Ed.* **2020**, *59*, 9377-9381; b) M. Zhu, J. Hu, Q. Lu, H. Dong, D. D. Karnaushenko, C. Becker, D. Karnaushenko, Y. Li, H. Tang, Z. Qu, J. Ge, O. G. Schmidt, *Adv. Mater.* **2021**, *33*, 2007497; c) Y. Dai, C. Zhang, W. Zhang, L. Cui, C. Ye, X. Hong, J. Li, R. Chen, W. Zong, X. Gao, J. Zhu, P. Jiang, Q. An, D. J. L. Brett, I. P. Parkin, G. He, L. Mai, *Angew Chem. Int. Ed.* **2023**, *62*, e202301192; d) H. Peng, C. Liu, N. Wang, C. Wang, D. Wang, Y. Li, B. Chen, J. Yang, Y. Qian, *Energy Environ. Sci.* **2022**, *15*, 1682-1693.

[21] H. Du, R. Zhao, Y. Yang, Z. Liu, L. Qie, Y. Huang, *Angew Chem. Int. Ed.* **2022**, *61*, e202114789.

[22] a) H. Li, C. Guo, T. Zhang, P. Xue, R. Zhao, W. Zhou, W. Li, A. Elzatahry, D. Zhao, D. Chao, *Nano Lett.* **2022**, *22*, 4223-423; b) H. Liu, J.-G. Wang, W. Hua, L. Ren, H. Sun, Z. Hou, Y. Huyan, Y. Cao, C. Wei, F. Kang, *Energy Environ. Sci.* **2022**, *15*, 1872-1881.

[23] X. Yang, J. Lv, C. Cheng, Z. Shi, J. Peng, Z. Chen, X. Lian, W. Li, Y. Zou, Y. Zhao, M. H. Rummeli, S. Dou, J. Sun, *Adv. Sci.* **2023**, *10*, 2206077.

[24] H. Liu, Q. Ye, D. Lei, Z. Hou, W. Hua, H. Yu, N. Li, C. Wei, F. Kang, J.-G. Wang, *Energy Environ. Sci.* **2023**, *16*, 1610-1619.

[25] J.-L. Yang, J. Li, J.-W. Zhao, K. Liu, P. Yang, H. J. Fan, *Adv. Mater.* **2022**, *34*, 2202382.

[26] a) H. Zhang, Y. Fang, F. Yang, X. Liu, X. Lu, *Energy Environ. Sci.* **2020**, *13*, 2515-2523; b) S. Jiao, J. Fu, M. Wu, T. Hua, H. Hu, *ACS Nano* **2022**, *16*, 1013-1024.

[27] Q. Zhang, Y. Ma, Y. Lu, Y. Ni, L. Lin, Z. Hao, Z. Yan, Q. Zhao, J. Chen, *J. Am. Chem. Soc.* **2022**, *144*, 18435-18443.

[28] M. Qiu, P. Sun, Y. Wang, L. Ma, C. Zhi, W. Mai, *Angew Chem. Int. Ed.* **2022**, *61*, e202210979.

[29] a) J. He, Y. Tang, G. Liu, H. Li, M. Ye, Y. Zhang, Q. Yang, X. Liu, C. Li, *Adv. Energy Mater.* **2022**, *12*, 2202661; b) C. Zhao, Y. Du, Z. Guo, A. Chen, N. Liu, X. Lu, L. Fan, Y. Zhang, N. Zhang, *Energy Storage Materials* **2022**, *53*, 322-330.

10.1002/anie.202403918

WILEY-VCH

RESEARCH ARTICLE

Entry for the Table of Contents

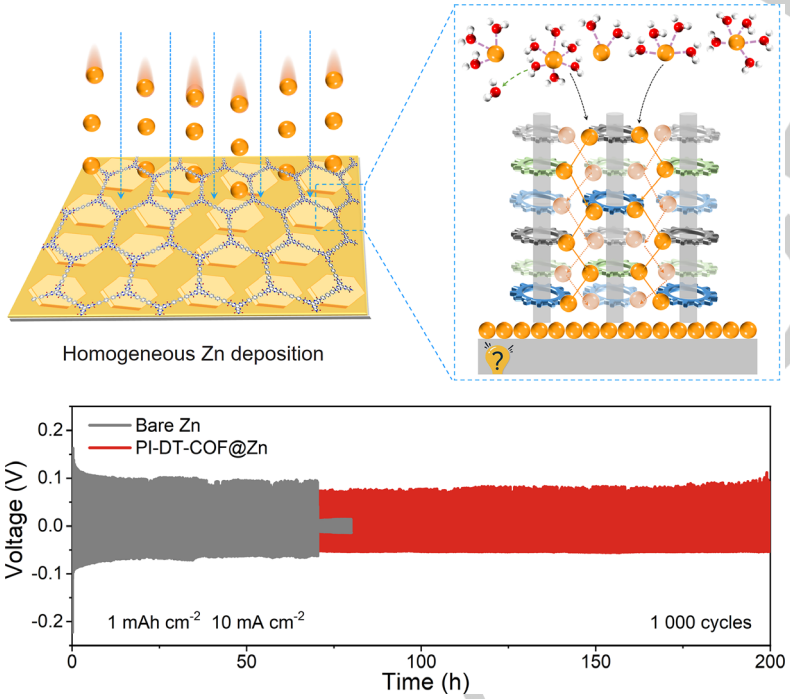

A series of anhydride-based covalent organic frameworks (i.e., PI-DP-COF and PI-DT-COF) with specifically designed zigzag hopping sites and zincophilic anhydride groups that can serve as desired platforms to investigate the related Zn^{2+} hopping/transfer, dendrite-inhibition, and plating/stripping behaviours as well as the interfacial interaction.